F. İnci / Hacettepe J. Biol. & Chem., 2022, 50 (2), 193-204

Research Article

Hacettepe Journal of Biology and Chemistry

journal homepage: www.hjbc.hacettepe.edu.tr

Bioinspired Material-Integrated Sensors for Improving Nanoplasmonic Characteristics

Nanoplazmonik Özelliği Geliştirmek için Biyoilhamlı Malzeme-Entegre Sensörler

Fatih Inci[1,2]

[1]UNAM–National Nanotechnology Research Center, Bilkent University, Ankara, Turkey.

[2]Institute of Materials Science and Nanotechnology, Bilkent University, Ankara, Turkey.

ABSTRACT

In this study, we demonstrated a nanoplasmonic-based sensor design, which was constructed with a bioinspired silk material and plasmonic materials (gold nanoparticles). We characterized this mutual integration at the molecular level by using Atomic Force Microscopy, Scanning Electron Microscopy, and also, the chemical composition was confirmed with Attenuated Total Reflectance-Fourier Transform Infrared Spectroscopy and X-Ray Photoelectron Spectroscopy analyses, along with contact angle measurements for evaluating hydrophilicity/hydrophobicity. Once a single layer of silk-gold nanoparticle mixture was accomplished, we serially applied an adlayer and plasmonic material to create more sensitive surfaces. Accordingly, we benchmarked the performance of this multi-layer sensor system, and observed ~6.8 times (or red-shifts from 7.93 nm to 12.90 nm) signal improvements compared to the one developed with a single layer. In sum, we here presented (i) a facile drop-casting method for developing a nanoplasmonic sensor design, (ii) the use of inexpensive off-the-shelf plastic as a substrate, (iii) easy-to-adapt strategy with standard spectrometer devices, and (iv) the need for minimum training for the proper use.

Key Words

Biosensor, nanoplasmonics, bioinspired materials, silk.

ÖZ

Bu çalışmada, biyoilhamlı ipek ve plazmonik malzemeler (altın nanoparçacıklar) ile oluşturulmuş nanoplazmonik-tabanlı bir sensör tasarımı geliştirilmiştir. Bununla birlikte, Atomik Kuvvet Mikroskobu, Taramalı Elektron Mikroskobu kullanarak moleküler düzeyde karakterize edilmiş ve kimyasal bileşim, hidrofiliklik/hidrofobiklik değerlendirmesi için temas açısı ölçümleriyle birlikte Zayıflatılmış Toplam Yansıma – Fourier Dönüşümlü Kızıl Ötesi Spektrometresi ve X-ışını Fotoelektron Spektroskopisi analizleriyle doğrulanmıştır. Tek bir ipek-altın nanoparçacık karışımı elde edildikten sonra, daha hassas yüzey ler oluşturmak için bir protein tabakası ve plazmonik malzeme sırasıyla yüzeye uygulanmıştır. Bu çok katmanlı sensör sisteminin performansı tek bir katman tarafından geliştirilen sistemle karşılaştırılmış ve ~6,8 kez (veya 7,93 nm'den 12,90 nm'ye sinyal kayması) sinyal iyileştirmesi gözlemlenmiştir. Özetle, burada (i) bir nanoplazmonik sensör tasarımı geliştirmek için yapılması kolay bir damla-döküm yöntemini, (ii) alt katman olarak, pahalı olmayan âtıl bir plastiğin kullanılmasını, (iii) standart spektrometrelere kolay adaptasyon stratejisini ve (iv) doğru kullanımı için en az seviyede eğitim gerektiği gösterilmiştir.

Anahtar Kelimeler

Biyosensör, nanoplazmonik, biyoilham malzemeleri, ipek.

Article History: Received: Dec 13, 2021; Revised: Jan 18, 2022; Accepted: Jan 28, 2022; Available Online: Feb 28, 2022.

DOI: https://doi.org/10.15671/hjbc.1035918

Correspondence to: Fatih Inci, UNAM–National Nanotechnology Research Center, Institute of Materials Science and Nanotechnology, Bilkent University, Ankara, Turkey.

E-Mail: finci@bilkent.edu.tr

INTRODUCTION

Biosensing has garnered significant attention in a myriad of areas, including clinical diagnostics [1], environmental monitoring [2], food analysis [3], and pharmaceutical studies [4]. This expansion has paved the way for the researchers to produce distinct biosensing strategies [5]; for instance, the electrochemical modality basically focuses on the redox reactions between the recognition element and the target analyte [6]. Since biological matrices have distinct pH values, ionic content and strength, this inherent property would potentially limit their utility, and therefore, they require multi-step washes to minimize the hindrance of biological matrix [7]. Mass-sensitive strategies, on the other hand, provide minute changes in the total mass of sensor by tracking oscillations or changes in surface stress through either depletion in the frequency, the bending of a cantilever or the other mass sensitive units [8,9]. Despite providing ultra-sensitivity—even down to a single molecule level [10,11] the proper operation of such systems requires an isolation unit to avoid any potential vibrations or temperature changes that impede the sensor performance significantly [12]. Hence, their deployment into clinical settings or research laboratories require more sophistication compared to the earlier sensor type. Moreover, optical systems provide a variety of modalities, such as fluorescent, absorbance, plasmonics, nanoplasmonics, Raman sensor, surface-enhanced Raman spectroscopy or surface-enhanced Raman scattering (SERS), whispering gallery mode, and so on. Among them, nanoplasmonics-stemmed strategies that utilize an electromagnetic field around nanostructured metal surfaces and/or nanoparticles, have exhibited quantitative and sensitive measurements [13–15]; however, they require sophisticated facilities for their proper fabrication. Although nanoparticle-based strategies have been employed in many studies, nanoparticle aggregation still constitutes a significant problem for the production of a multi-layer sensor.

While detecting an analyte, all the aforementioned biosensing strategies need to be evaluated comprehensively by considering the analytical performance [13]. For instance, one of the most attractive features is to provide sufficient analytical performance compared to the existing methods in practice [16], and minimize the current challenges in adapting them into the clinical and research laboratory settings [16,17]. Although biosensing strategies provide notable improvements in this regard, there are some points need to be considered before their adaptation. As an example, the user-interface should be facile, and therefore, the end-user would require only minimal training for the proper operation [13]. The sensor and/or read-out device cost is one of the major considerations while producing a biosensing system, and their wide expansion would be critically reliant on the cost-related issues [18]. In addition to its expansion, analytical performance needs to be performed to benchmark the performance of biosensors. Sensitivity is one of the most studied parameters to improve these systems, and also some labeling materials have been utilized to further enhance the response signal than that of the bare surface [19]. Labeling step, however, increases more complexity owing to new interventions, such as the additional sampling and washing steps, and most importantly, it requires significant efforts to passivate the surface for protecting or minimizing false positive results. All these pivotal parameters need to be implemented in designing a new sensor before its deployment into a specific field or setting.

In this study, we designed a nanoplasmonic sensor through the integration of a bioinspired material (silk) on an off-the-shelf material having nanoperiodic structures to increase surface area, thereby improving the detection of analytes. In addition to a single layer of silk and AuNPs, we benchmarked the sensor performance by inserting one layer of silk as adlayer and another layer of AuNPs as plasmonic layer. Moreover, we continued this metamaterial design with five layers of such modifications in total. As plasmonic sensors are majorly evaluated by altering the refractive index of surrounding medium, we have here applied different concentrations of glycerol as a model analyte, and also evaluated the signal enhancements in the five layers of modifications compared to the bare (single layer) surface. All the characterization parameters including morphology, nanoperiodicity, chemistry, and hydrophilicity/hydrophobicity were assessed comprehensively with the molecular techniques as elaborated below.

MATERIALS and METHODS

Materials

Silk fibroin solution (50 mg/mL) was supplied from Bugamed Biyoteknoloji ARGE. Sodium citrate dihydrate and Gold (III)chloride trihydrate ($HAuCl_4 \cdot 3H_2O$) and methanol (99.7%, Sigma-Aldrich) were purchased from Sigma-Aldrich. Phosphate Saline Buffer (PBS) tablets were

obtained from Biomatik. Glycerol (85%) was purchased from Isolab Chemicals. The other organic solvents including ethanol (96%, Soltek), isopropanol alcohol (99.5%, Lobal Chemie), and acetone (99.5%, Birpa) were purchased from the companies stated here. All chemicals were used without further purification, and deionized water was used throughout. Optical DVD discs (Sony) were used as plastic surfaces (PS).

Gold nanoparticle synthesis

Gold nanoparticles (AuNPs) were synthesized through a seeding reaction. For this purpose, the seeding solutions were first prepared by the citrate reduction. Briefly, 90 mL of sodium citrate solution (containing 60 mg of sodium citrate dihydrate) were heated to boil for 10 minutes under vigorous stirring. Then, 6 mg of $HAuCl_4 \cdot 3H_2O$ were introduced to the solution and kept boiling for 30 minutes. The solution was allowed to cool down to 90 °C. Subsequently, 25 mM of sodium citrate (3 mL) and 1 mM $HAuCl_4 \cdot 3H_2O$ solution (3 mL) were added to the seed solution, and the boiling was continued for 30 minutes. Finally, the solution was allowed to cool down to room temperature, and stored at +4 °C until the use.

Preparing plastic surfaces

Commercial optical discs were used as sensor substrates due to their nanoperiodicity, potentially increasing the surface area [20]. Principally, optical discs are constructed in a multi-layer structure, consisting of a top plastic surface, metal-coating, photoresist layers, surface grating, and polycarbonate-plastic layers [21]. Herein, the transparent PS was prepared by removing the coating layer on the optical disc along with undesired metal-coating and photoresist layers through physical and chemical processes. Briefly, (1) the top coating layer of optical disc was removed using a knife; (2) the metal-coating was removed using an air pump; (3) the surface was then cleaned using a mixture of ethanol (EtOH) and methanol (MetOH) (1:1: v:v), followed by a washing step with distilled water; and (4) finally, the surface was etched with a mixture of acetone and isopropanol (1:4; v:v) for 60 seconds to generate the nanoperiodic structures more efficiently. (5) Once the etching step was accomplished, the surface was washed with distilled water, and (6) the resultant optical discs (PS) were cut into 1.5 × 1.5 cm^2 squares with scissors for the experiments.

Modification of plastic surfaces

The PS materials were first modified with a mixture of silk and AuNPs, and this layer was defined as "single layer (SL)". Briefly, 2 mL of AuNP solution was centrifuged, and 1.5 mL of supernatant was removed to concentrate AuNPs in the solution. The concentrated AuNP solution was used to dilute the stock solution of silk in a 1:50 ratio, and this resulted in 1 mg/mL of silk-AuNPs solution (excluding the mass of nanoparticles). This solution was kept at +4 °C for 2 days. Once this storage period ended, 250 µL of solution was drop-casted onto the surface and spread properly to cover the PS material, followed by an air-drying process at room temperature. The surface was then treated with 70% of methanol solution and incubated for 10 minutes. Finally, the PS modified with SL was rinsed with distilled water and dried using an air-pump system. Layer-by-layer modification with adlayer (silk) and plasmonic metal particles (AuNPs) were applied through the same procedure. In this process, silk solution (250 µL of 1 mg/mL, without AuNPs) was drop-casted onto the surface, and similarly, an air-drying process was applied at room temperature. Likewise, the surface was treated with 70% of methanol solution and incubated for 10 minutes, and this process was defined as the second layer (SL + silk). For the third layer (SL + silk + AuNPs) modification, we applied 250 µL of aqueous gold nanoparticles to this surface through drop-casting, thereby properly spreading the nanoparticle solution to cover the earlier surface, and this step followed to the treatment with 70% of methanol solution and incubating it for 10 minutes. The fourth layer (SL + silk + AuNPs + silk) and fifth layer (SL + silk + AuNPs + silk + AuNPs) were prepared by following the same procedure that was applied for the second and third layer , respectively.

SEM imaging

The topographical analysis was carried out *via* Scanning Electron Microscope (SEM) (FEI Quanta 200 FEG). The PS and the modified surface (SL) were coated with 10 nm of Au/Pd, and these samples were then placed to the holder for the imaging studies.

AFM study

For another topography analysis, Atomic Force Microscope Analysis (AFM) (Asylum, Oxford Instrument, U.K.) was carried out using Nanosensors PPP-NCHR tip with 42 N m^{-1} force constant on AC Air Topography. The tip was landed on the sample until Z voltage value around 70V, and the imaging process was applied with 0.6 Hz scanning rate. The images were analyzed using Gwyddion without any data manipulations, including filters or smoothing operations.

Attenuated total reflectance-Fourier transform infrared spectroscopy (ATR-FTIR) Analysis

In this analysis, we examined the integration of silk and AuNPs to the PS material. In this regard, we evaluated the bare PS, silk material on a glass surface, silk material on the PS, and silk-AuNPs on the PS. Before the analysis, the sampling area was cleaned with isopropyl alcohol, and the background (air) was measured to minimize any environmental influences during the measurements. The sensor surface was then placed on to the sample module containing a diamond probe, and it was scanned from 400 to 4000 cm^{-1} of wave numbers to measure total absorbance at specific wave numbers, specifying the resultant chemical groups on the surface.

Contact Angle Experiments

We measured contact angles on the surfaces of bare PS, silk on the PS, and silk-AuNPs on the PS material using the Contact Angle Measurement System (Dataphysics, OCA 30, Filderstadt, Germany). In this process, we dropped a 2 µL of ultrapure water to the surfaces, and recorded the resultant angles using an in-house software.

X-Ray Photoelectron Spectroscopy (XPS) measurements

Here, we examined the formation of SL on the PS surface through the XPS analysis. The PS surface without any modifications was used as a control. The experimental conditions and arrangements were set on the XPS system (Thermo Fisher K-Alpha), and all the parameters and data collection were acquired from the software (Thermo Advantage).

Spectrometric Measurements

The sensor surfaces were placed in a 12-well plate, and all the measurements were performed using a standard microplate reader (SpectraMax M5, San Jose, CA, U.S.A.) within a wavelength range of 400-750 nm along with 1 nm of the step size. All conditions such as air, water, and various glycerol concentrations (1-70 %) were applied to the sensors inside the wells. Between each measurement, the sensor surfaces were properly washed with distilled water.

Data Analysis

The peak wavelength and extinction intensity were presented by calculating the centroid values within the range from 500 nm to 600 nm, where the spectral peak points located. In this process, we utilized OriginPro software (Northampton, Massachusetts, USA). Considering the finite resolution of the instrument, the intensity values were rounded to the third decimal digit, and the peak wavelength values were rounded to the first decimal digit. In addition, the data normalization process was performed through the function of NORM.DIST of Microsoft Excel.

RESULTS and DISCUSSION

In this study, silk material was chosen to construct the sensor since it provides notable features, including biocompatibility, low-cost, mechanically robustness/flexibility, and eco-friendly, as well as it can be processed into a myriad of forms such as films, opals, and gels [22–24]. All these features make silk as a unique material for sensor designing. In particular, the biocompatibility and mechanically reliable fashions would expand its applicability in wearable sensing strategies, thereby accelerating the continuous monitoring of biological analytes. Briefly, in this study, the formation of nanoplasmonic sensor included (i) the coating of adlayer and plasmonic metal particles on a PS material through a mixture of silk and AuNPs (1 mg/mL)—defined as single layer (SL) that creates the first layer of sensor surface. Later, the PS with SL coating were modified with silk and AuNPs sequentially in order to generate five layers of adlayer-plasmonic materials in total (Figure 1a). In this fabrication strategy, we first characterized the surface parameters of PS, including their 3-D structures, chemical composition, and surface properties. In this manner, we imaged the PS using both SEM and AFM (Figure 1b-g). Per the images, the PS had continuous nanograting structures with ~740 nm of periodicity, ~500 nm of width, and ~150 nm of height (Figure 1d). This nanostructure expanded the total area ~40% more than that of a flat surface, enabling the more binding spots for AuNPs to silk materials. Another examination was performed on the coating of SL to the PS, and we observed that the SL coating partially followed the nanoperiodicity of the PS, yet created mostly smooth surface by reducing the roughness of ~7 nm (Figure 1g).

Moreover, we evaluated the formation SL through a mixture of silk and AuNPs on a flat surface (glass) and the PS *via* ATR-FTIR measurements as stated in the literature [25–27]. Since different chemical groups and bonds provide intrinsic reflections in the FTIR spectrum, this information has enabled us understanding the success of surface chemistry on the surface. We here evaluated four different experimental sets: (i) bare PS,

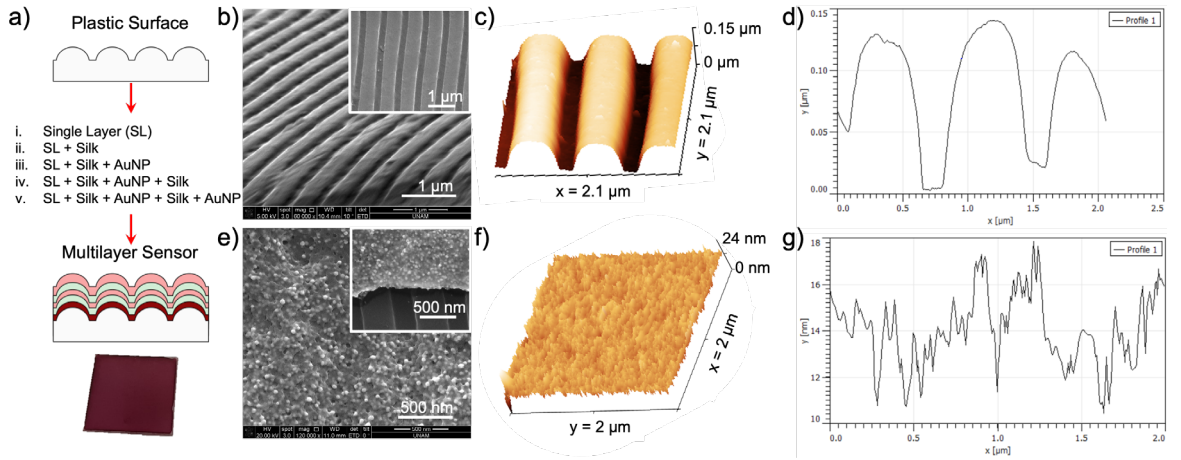

Figure 1. The fabrication and surface characterization of the sensor. a) Plastic surface consists of a nanoperiodic structure, which is modified with (i) a mixture of silk and AuNP, and (ii-v) serially coated with silk and AuNP layers, thereby forming a layer-by-layer nanoplasmonic sensor structure. b) An SEM image of the plastic surface, and the inset image provides more details of the nanoperiodic structures on the PS (scale bars represent 1 µm). c-d) An AFM image demonstrates the nanoperiodic structures with grooves having ~740 nm of periodicity, ~500 nm of width, and ~150 nm of height. e) An SEM image is taken after the layer-by-layer modification on the sensor.. The inset image presents both the coated and nanoperiodic structure (scale bars represent 500 nm). f-g) An AFM image displays the morphology of sensor after the layer-by-layer modification. The roughness of the sensor surface reduces down to ~7 nm, stating smoother surface after this modification.

(ii) silk on the glass, (iii) silk on the PS, and (iv) SL (silk-AuNP) on PS. Briefly, the bare PS provided three distinct absorbance peaks, and the intensity band appearing in the region of 1465.8 cm^{-1} was assigned to C-H bending vibrations of alkanes and alkenes. The second peak at 1502.5 cm^{-1} exhibited at the C-C aromatic skeletal vibrations. The third peak located at the region 1600 cm^{-1} that was designated to C=C stretching vibrations (Figure 2a). While comparing the silk modification on glass and PS, we observed the peaks locating at same locations, yet different intensity rates. For instance, the intensity at 1512.2 cm^{-1} was designated to N-H deformation (Amide II) vibrations, and also, C=O stretching (Amide I) bond was observed at 1618.3 cm^{-1} (Figure 2a). Consequently, silk modification on PS provided ~5 times greater intensity than that of silk on glass experimental set, which was possibly caused by enhancing surface area. Once AuNP modification was accomplished, we observed some slight changes at the signals caused by silk material, as well as found a distinct peak at 1504.4 cm^{-1}, matching the peak location of the bare PS. Overall, ATR-FTIR analysis pointed out the success of surface chemistry, as well as it presented signal enhancements at the intrinsic chemical groups due to the surface area expansion. In addition, through the contact angle measurements, we assessed the hydrophilicity/hydrophobicity of the PS before and after the surface modification with silk and the formation of SL were accomplished (Figure 2b). The bare PS provided 74.4° ± 3.2°, whereas the surface modifications with silk and SL provided more hydrophilic surfaces with the contact angles of 61.2° ± 3.0° and 52.4° ± 3.1°, respectively. Overall, this observation stated the successful integration of silk and AuNPs.

We later performed an analysis of XPS to characterize the SL applied onto the PS material. Basically, XPS utilizes to determine the elemental composition and chemical state in the material through photoelectric effect. The chemical composition of the bare PS was examined with C1s, N1s, O1s, and Au. The bare PS provided distinct peaks associated with C-C at 283.55 ± 0.202 eV, C-O at 284.99 ± 1.189 eV, and C=O 286.85 ± 0.015 eV—major chemical groups in the polycarbonate structure of the bare PS (Figure 3a). We also observed a small, yet a sharp peak corresponding to the polymeric backbone of PS, ***i.e.,*** C-H at 284.671 ± 2.081 eV. Besides, the bare PS provided additional peaks in N1s and O1s studies, corresponding to imine bond at 398.73 ± 0.004 eV and C-O at 530.40 ± 0.01 eV, respectively (Figure 3b-c). While examining for Au, no specific peaks were observed for the bare PS (Figure 3d). Once the SL was accomplished on the bare PS surface, we observed same chemical bonds in C1s plot with varying binding energies, which might be caused by the carbon-related bonds in silk structure (Figure 3e). In addition, the intensities corresponding to the binding energies altered. For instance, in

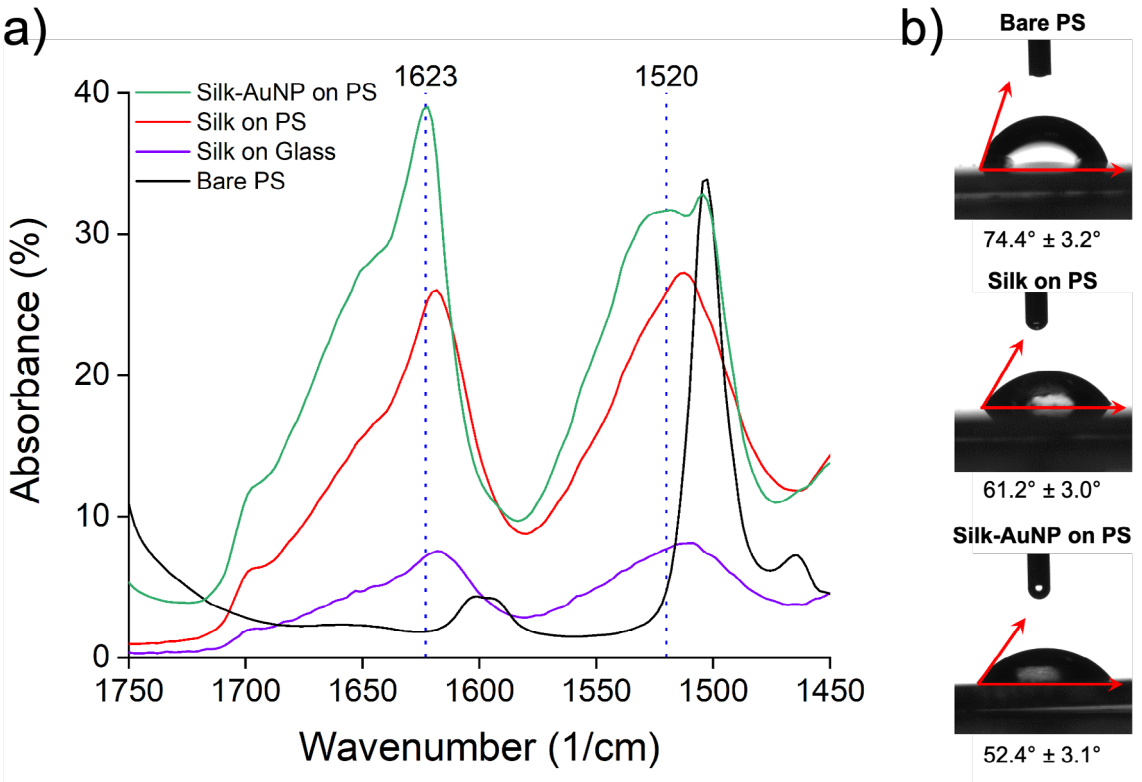

Figure 2. Characterization of the surfaces. a) ATR-FTIR characterization is applied to evaluate the chemical bond formation on different experimental sets. b) Hydrophilicity/hydrophobicity characteristics of different surfaces are examined with the contact angle measurements.

C1s plot, we observed C=O bond at the binding energy of 287.77 ± 0.038 eV and the intensity level associated with C=O reduced from 5252.79 a.u. to 4651.1 a.u. after the modification. Likewise, C-O bond was observed at 286.06 ± 1.195 eV along with a reduction in the intensity from 6205.36 a.u. to 4935.35 a.u. On the other hand, C-C bond was observed at 284.46 ± 0.104 eV, and its intensity increased from 4783.22 a.u. to 5620.87. Furthermore, C-H bond appeared obviously at 285.61 ± 0.264 eV after the modification, and the intensity was around 3 times more than that of the bare PS. The intensity increments in C-C and C-H bonds would be expected since silk is in amino acid structure, and the C-C and C-H are the major components of the amino acid backbone. Comparing it with the bare PS, the surface with the SL modification provided comparable bonds at the N1s and O1s spectrum, and similarly, their binding energies were different, pointing out the binding of silk molecules to the bare PS. In the N1s plot, the corresponding intensity changed from 84346.89 a.u. to 7764.48 a.u.; however, we did not observe such changes in the O1s plot. Moreover, silk-AuNP modification was observed with two peaks associated with Au ($4f_{7/2}$) and Au ($4f_{5/2}$) at the binding energies of 87.67 ± 0.015 eV and 84.01 ± 0.012 eV, respectively (Figure 3h); however, there were no Au-related peaks on the bare surface. Consequently, three distinct characterization methods (ATR-FTIR, contact angle, and XPS) clearly indicated the successful integration of SL (silk-AuNPs) with the bare PS.

To evaluate the performance of sensor with SL, we first designed experimental sets including the measurements in air and water conditions, as well as tested the sensor response over glycerol solutions with distinct refractive index (RI) values (Figure 4). In air measurements, we observed that the nanoplasmonic data provided higher intensity compared to the other sets, reaching up to 0.628 of extinction intensity at a peak wavelength of 540 nm (Figure 4a). The measurements in water provided the minimum intensity at a peak wavelength of 529 nm; yet the spectra provided a clear nanoplasmonic curve. Similarly, we observed such gaussian curves in glycerol experimental sets, and the sensor responded to all the solutions with different RI values.

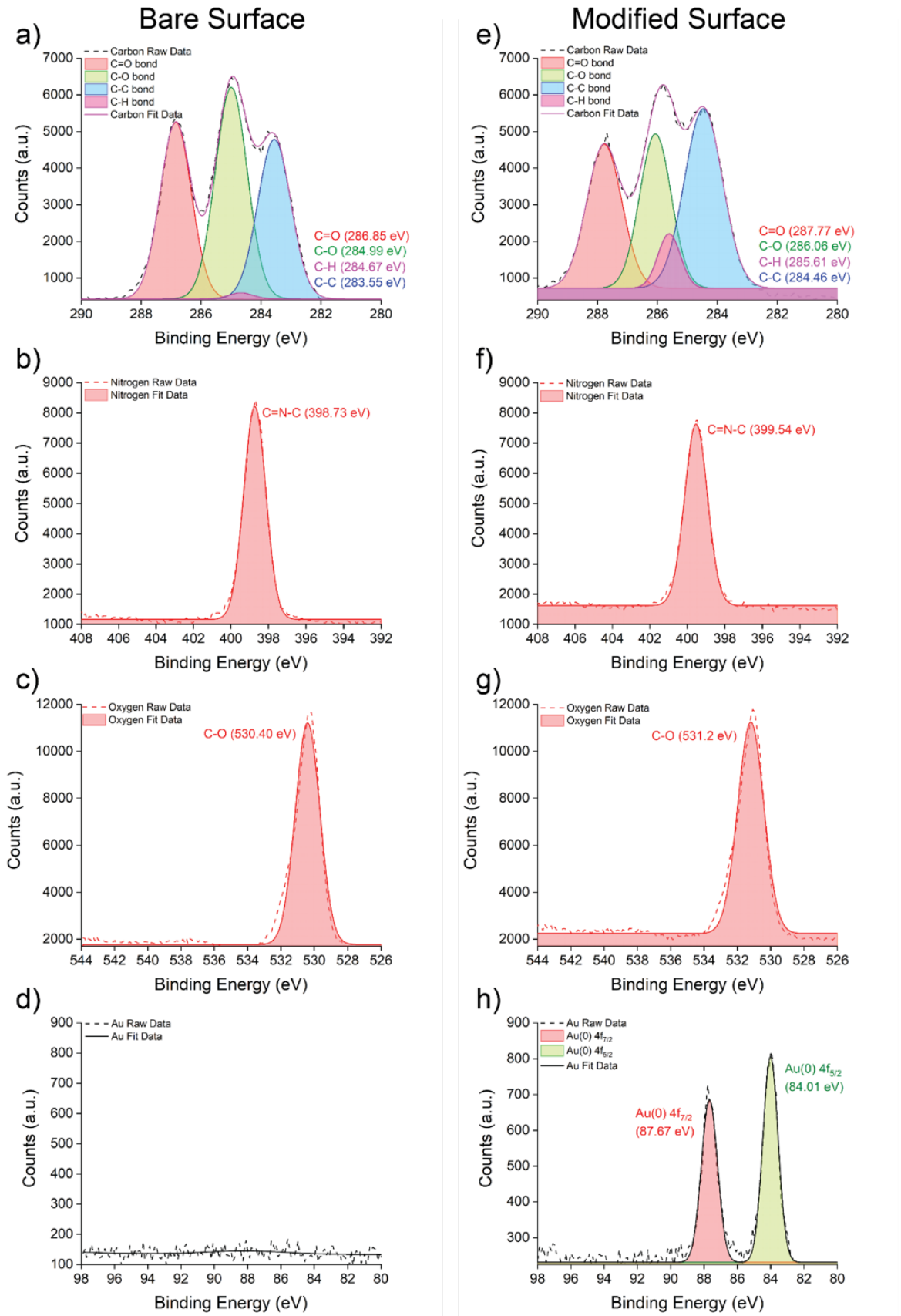

Figure 3. The XPS analysis. (a-d) The bare PS and (e-h) the modified surfaces (SL coated PS material) are examined through C1s, N1s, O1s, and Au4f XPS spectra. The corresponding chemical groups along with their binding energies are stated on the plots.

This response curve was further evaluated in terms of glycerol concentrations *versus* the resultant peak wavelength values. The heatmap plot indicates that the peak wavelength values changed due to the surrounding medium with distinct RI values (Figure 4b), and we also observed linear increments in the regime of glycerol concentrations, reaching up to 536.9 nm (Figure 4c).

To understand the performance of this sensor formation, we then calculated two major parameters: (i) RI sensitivity and (ii) figure-of-merit (FOM) [28] . Basically, surface plasmons are greatly sensitive to the RI of the surrounding medium. In glycerol experiments, we observed red-shifts in the peak wavelength values, and then divided the magnitude of this shift by the alteration in RI. This calculation is defined as the RI sensitivity ($\frac{\Delta\lambda}{\Delta n}$), and the sensor provided ~69.03 nm/RI. The FOM of a plasmon resonance is defined as the ratio between the RI sensitivity and the width of the resonance peak ($FOM = \frac{RI\ sensitivity}{FWHM}$). Accordingly, we calculated all these values for each glycerol concentration (Table 1). As a result, higher values of the FOM indicate better sensor performance, thereby stating our detection limit could be further tuned with the solutions having from 1.334 to 1.339 RI—well matching with biological matrices such as serum, urine, and plasma [29,30].

In addition, we formed the multi-layers of silk and AuNPs onto the surface of SL, and measured their nanoplasmonic responses in air and various concentrations of glycerol solutions (Figure 5a). Adding more layers to the SL led to an increase in the extinction intensity of the sensor clearly. For instance, the second layer including the SL and silk resulted in 0.604 a.u. of extinction

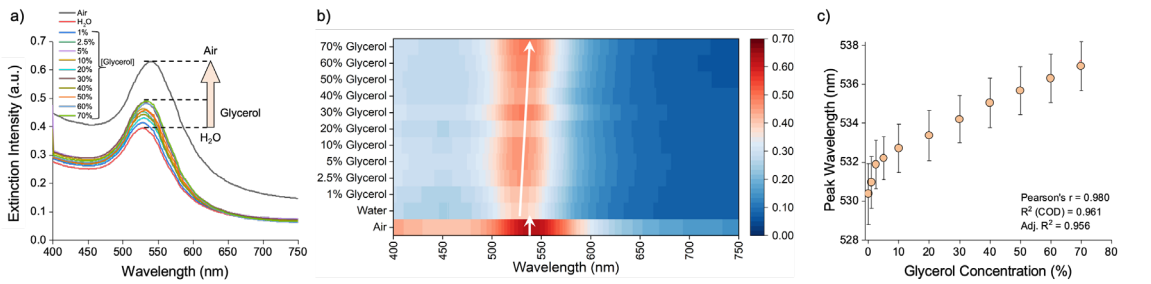

Figure 4. Benchmarking the nanoplasmonic signals for the sensor with a single layer (SL) of silk-AuNP mixture. a) The sensor with SL is evaluated with different conditions, such as air, water, and various concentrations of glycerol solution ranging from 1% to 70%. b) The heatmap plot represents the nanoplasmonic signals as the responses to different glycerol concentrations. White arrows state the peak wavelength value for each surrounding medium. c) The peak wavelength values (centroid values) of the sensor are plotted in the presence of different glycerol solutions.

Table 1. Figure-of-merit (FOM) calculation of the sensor at different glycerol concentrations (FWHM represents full width at half maximum of the curves).

Glycerol Concentrations (%)	RI	FWHM	FOM
0	1.333	36.02	1.92
1	1.334	35.70	1.94
2.5	1.336	35.72	1.93
5	1.339	35.70	1.93
10	1.345	37.41	1.85
20	1.358	37.56	1.84
30	1.371	37.22	1.86
40	1.384	37.35	1.85
50	1.398	39.95	1.73
60	1.413	40.48	1.71
70	1.428	40.43	1.71

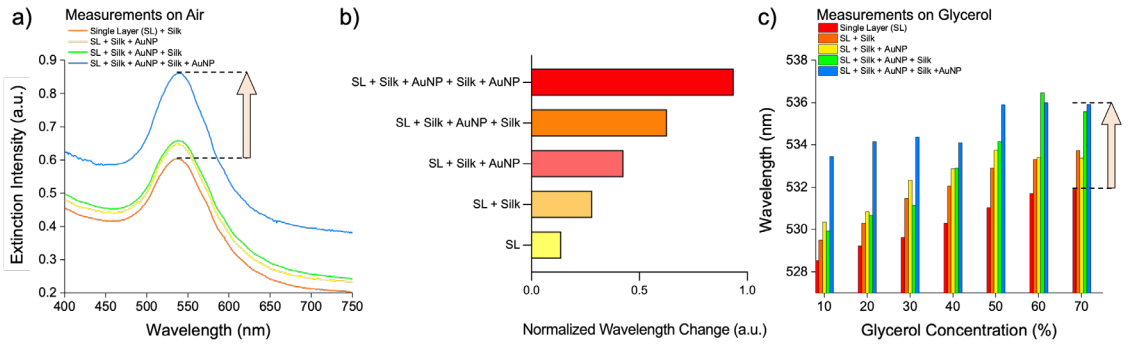

Figure 5. Assessing the performance of nanoplasmonic sensor with the layer-by-layer modification. a) The nanoplasmonic signals of each modification step are measured in air condition. b) Normalized data is demonstrated for each condition. c) A variety of glycerol concentrations ranging from 10 % to 70 % is applied to these sensors with different coatings, and the nanoplasmonic signal (peak wavelength) is measured single layer (SL) and multi-layer coatings.

intensity at ~536 nm of peak wavelength; the third layer formed by the SL, silk, and AuNPs led to 0.649 a.u. of extinction intensity at 537.2 nm of peak wavelength; the fourth one including the SL, silk, AuNPs, and silk resulted in 0.658 a.u. of extinction intensity at 537.4 nm of peak wavelength; and the last one defined as the SL, silk, AuNPs, silk, and AuNPs provided 0.861 a.u. of extinction intensity at 538.4 nm of peak wavelength. Moreover, considering the peak wavelength value of AuNP as ~520 nm, we calculated the wavelength changes between different layers. We observed that the SL provided 7.93 nm of red-shifts, and this continued to proportional to each modification, resulting in 12.90 nm of red-shifts. Then, we normalized the data of peak wavelength changes to understand the fold changes in different layers (Figure 5b). Per the normalization analysis, the SL provided 0.138 a.u., whereas this value increased up to 0.937 a.u. at the final format, pointing out that ~6.8 times increments. We then assessed the sensor performance with different layers at different glycerol concentrations (Figure 5c). Per the results, each experimental set responded an increase in the peak wavelength value, and in most of the sets, we observed approximately ~4 nm of increments in the peak wavelength values of SL and the surface modified with five layers at the highest concentration of glycerol.

On the other hand, reproducibility is one of the critical parameters while producing polymers and applying them into layer-by-layer formations. In this regard, polymer concentration, the quality of polymer batches, and storage/application conditions (temperature, solvent, and pH) would be pivotal while preparing the layers. In this study, we have constructed the sensor with silk-AuNP mixture (SL) and sequentially accommodate the layers of silk and AuNPs. Moreover, all the layers demonstrated here have provided highly stable features along with reproducible signals while applying very distinct medium such as water, methanol, and various concentrations of glycerol. In particular, glycerol solutions were applied sequentially after washing the surfaces with water. At different layers of the sensor surfaces (SL to 5-layer surface), we did not observe any challenges on the chemical stability, and as shown in Figure 5c, the performance of sensor surface with different layers did not change during this experiment.

Table 2. Comparing the platforms in terms of the sensing methods, modification features, polymer substrate, fabrication, sensitivity, signal enhancer molecules, and signal increments.

Sensing Strategy	Layer-by-layer Modification	Polymer/ Biological Substrate or Anchors	Fabrication	Sensitivity	Enhancer Molecule and Strategy	Signal Increment	Ref.
Localized Surface Plasmon Resonance	Yes	Poly-L-lysine	Drop-casting	10 IU/ mL (virus detection)	Sandwiching viruses between AuNPs	1.53 - 1.77 times	[14]
Photonic Crystal Enhanced Microscopy (PCEM)	Yes	Anti-IgG	Clean room facility and advanced equipment	Single nanoparticle	Au nanorods	Not Reported	[31]
Surface Plasmon Resonance	Yes	Self-assembled monolayers and antibodies	Surface modification to immobilize antibodies	LOD (without AuNP): 100 ng/L LOD (with AuNP): 10 ng/L	AuNPs	10 times	[32]
Localized Surface Plasmon Resonance	Yes	Silk	Drop-casting	RI sensitivity: 69.03 nm/RI FOM: up to 1.94 (Bulk sensitivity with glycerol)	Silk and AuNP mixture and their sequential coatings	~6.8 times	This study

CONCLUSION

In this study, we developed a nanoplasmonic sensor consisting of a bioinspired material and AuNPs, and all these materials were constructed properly on a PS surface containing a nanoperiodic structure in order to enhance the surface area. Increments on the surface area would potentially enable to detect more molecules, thereby increasing the sensitivity. In addition, we not only expanded the surface area up to 40% of increment, and also, provided a layer-by-layer construction of adlayer (silk) and nanoplasmonic material (AuNPs), along with five layers of this construction in total. Per the characterization results, AFM and SEM studies demonstrated explicitly that the surface roughness (down to ~7 nm) was altered once the formation of SL was achieved. Second, the SL construction enabled more hydrophilic surface down to 52.4° ± 3.1° of contact angle, and this was further characterized with ATR-FTIR and XPS analyses. Chemical compositions developed on the PS material were successfully demonstrated with the changes at binding energies and their intensities for C1s, N1s, O1s, and Au4f. Since nanoplasmonic sensors are evaluated with the response signals against the refractive index changes, we have assessed the sensor with SL by applying various concentrations of glycerol solutions (1%-70% of glycerol having RI values ranging from 1.333 to 1.428 of RI in the surrounding medium). After accomplishing the signal changes on the sensor, we further benchmarked the response signals on the multi-layer formulation of adlayers and plasmonic materials. Per the results, the nanoplasmonic signal was improved by ~6.8 times (or red-shifts from 7.93 nm to 12.90 nm) compared to the one developed with a SL only (considering that AuNPs without silk material provided a resonance at ~520 nm). Here, we demonstrated the development of a nanoplasmonic sensor platform along with easy-to-use, reliable, and sensitive fashions (~69.03 nm/RI), as well as improved the sensing capability with a facile construction strategy.

In addition, we here presented a comparison table focusing on distinct parameters, including sensing method, modification strategy, polymeric substrate, fabrication, sensitivity, enhancing molecule and signal increments (Table 2). Since this paper focuses on nanoplasmonics, especially localized surface plasmon resonance (LSPR), we assessed these features with the platforms having closer properties. For instance, the researchers denoted an unconventional strategy, where they captured viruses on an antibody-coated AuNP surface, and then, sandwiched these viruses with another set of antibody-AuNP conjugates [14]. Although this mutual integration resulted in 1.53 - 1.77 times signal increments, our current study provided higher signal increments (~4 times higher) than this study. In another research, Photonic Crystal Enhanced Microscopy (PCEM) was applied to detect single nanoparticles [31]. In this approach, the sensor surface was a nanoperiodic photonic crystal (PC) array. The researchers then introduced AuNPs to the PC surface and scanned the entire area. Despite its notable sensitivity, the fabrication of such sensors is costly and challenging, hence requiring sophisticated instruments, facilities, and strategies, such as deep-UV lithography and reactive ion etching. In our design, the fabrication of one single sensor provides an inexpensive and very facile features (drop-casting only), and the total material cost (PL (5 cent), silk (50 cents), and gold nanoparticles (10 cents)) is less than $1. On the other hand, surface plasmon resonance (SPR)-stemmed strategies were also utilized with signal enhancer molecules, such as AuNPs [32]. In this manner, the SPR sensor was decorated with self-assembled monolayers (SAMs) to immobilize antibodies, and the researchers then benchmarked the sensor performance in the presence or absence of AuNPs. Through this strategy, the sensor signal was improved 10 times. However, utilizing harsh chemistry conditions to develop the SAM would potentially hamper the applicability of this sensor in biomedicine field, especially integrating sensors to the wearable tools. Silk material is a biocompatible and bioinspired polymer, hence broadening its utility in such fields as well. Moreover, the presented sensor was measured using a standard spectrometer, which would potentially expand its applicability to multi-laboratory settings, as well as this would minimize the need for extensive training for the end-users. Since the production was so simple, the read-out mechanism would be easily transferred to a hand-held device, which would further reduce the need for a bench-top system and the device cost as well. Moreover, we anticipate that such a system would be more beneficial with the integration of smart materials for adapting new features such as dynamic responses against an external stimulus [33], and also with the implementation of microneedles that would enable both sampling and sensing characteristics on the same device [34].

Acknowledgments

Dr. Fatih Inci gratefully acknowledges the support from TÜBİTAK 2232-International Fellowship for Outstanding Researchers (Project No: 118C254), TÜBİTAK 3501-Career Development Program (CAREER) (Project No: 120Z335), and Turkish Academy of Sciences - Outstanding Young Scientists Award Program (TÜBA-GEBİP). This publication has been produced benefiting from the 2232 International Fellowship for Outstanding Researchers Program of TÜBİTAK (Project No: 118C254). However, the entire responsibility of the publication/paper belongs to the owner of the publication/paper. The financial support received from TÜBİTAK does not mean that the content of the publication is approved in a scientific sense by TÜBİTAK. This work was supported by the BAGEP Award of the Science Academy. Dr. Inci also acknowledges the helpful discussions with Ms. Esma Derin.

References

1. Y. Saylan, Ö. Erdem, S. Ünal, A. Denizli, An alternative medical diagnosis method: Biosensors for virus detection, Biosensors. (2019). https://doi.org/10.3390/bios9020065.
2. S. Leonardo, A. Toldrà, M. Campàs, Biosensors based on isothermal DNA amplification for bacterial detection in food safety and environmentalmonitoring, Sensors (Switzerland). (2021). https://doi.org/10.3390/s21020602.
3. S. Akgönüllü, H. Yavuz, A. Denizli, M. García, A. Castro Grijalba, Development of Gold Nanoparticles Decorated Molecularly Imprinted–Based Plasmonic Sensor for the Detection of Aflatoxin M1 in Milk Samples, Chemosens. 2021, Vol. 9, Page 363. 9 (2021) 363. https://doi.org/10.3390/CHEMOSENSORS9120363.
4. L. Qian, S. Durairaj, S. Prins, A. Chen, Nanomaterial-based electrochemical sensors and biosensors for the detection of pharmaceutical compounds, Biosens. Bioelectron. (2021). https://doi.org/10.1016/j.bios.2020.112836.
5. Y. Saylan, Ö. Erdem, F. Inci, A. Denizli, Advances in biomimetic systems for molecular recognition and biosensing, Biomimetics. (2020). https://doi.org/10.3390/BIOMIMETICS5020020.
6. E. VanArsdale, J. Pitzer, G.F. Payne, W.E. Bentley, Redox Electrochemistry to Interrogate and Control Biomolecular Communication, IScience. (2020). https://doi.org/10.1016/j.isci.2020.101545.
7. G.A. Akceoglu, Y. Saylan, F. Inci, A Snapshot of Microfluidics in Point-of-Care Diagnostics: Multifaceted Integrity with Materials and Sensors, Adv. Mater. Technol. (2021). https://doi.org/10.1002/admt.202100049.
8. B.O. Alunda, Y.J. Lee, Review: Cantilever-based sensors for high speed atomic force microscopy, Sensors (Switzerland). (2020). https://doi.org/10.3390/s20174784.

9. J. Mouro, R. Pinto, P. Paoletti, B. Tiribilli, Microcantilever: Dynamical response for mass sensing and fluid characterization, Sensors (Switzerland). (2021). https://doi.org/10.3390/s21010115.
10. A.K. Naik, M.S. Hanay, W.K. Hiebert, X.L. Feng, M.L. Roukes, Towards single-molecule nanomechanical mass spectrometry, Nat. Nanotechnol. (2009). https://doi.org/10.1038/nnano.2009.152.
11. Y. Saylan, A. Denizli, Fundamentals and Applications of Molecularly Imprinted Systems, Molecular Imprinting for Nanosensors and Other Sensing Applications, Elsevier, 2021: pp. 1–17. https://doi.org/10.1016/B978-0-12-822117-4.00001-0.
12. F. Inci, C. Filippini, M. Baday, M.O. Ozen, S. Calamak, N.G. Durmus, S.Q. Wang, E. Hanhauser, K.S. Hobbs, F. Juillard, P.P. Kuang, M.L. Vetter, M. Carocci, H.S. Yamamoto, Y. Takagi, U.H. Yildiz, D. Akin, D.R. Wesemann, A. Singhal, P.L. Yang, M.L. Nibert, R.N. Fichorova, D.T.Y. Lau, T.J. Henrich, K.M. Kaye, S.C. Schachter, D.R. Kuritzkes, L.M. Steinmetz, S.S. Gambhir, R.W. Davis, U. Demirci, Multitarget, quantitative nanoplasmonic electrical field-enhanced resonating device (NE2RD) for diagnostics, Proc. Natl. Acad. Sci. U. S. A. (2015). https://doi.org/10.1073/pnas.1510824112.
13. F. Inci, Y. Saylan, A.M. Kojouri, M.G. Ogut, A. Denizli, U. Demirci, A disposable microfluidic-integrated hand-held plasmonic platform for protein detection, Appl. Mater. Today. (2020). https://doi.org/10.1016/j.apmt.2019.100478.
14. F. Inci, M.G. Karaaslan, A. Mataji-Kojouri, P.A. Shah, Y. Saylan, Y. Zeng, A. Avadhani, R. Sinclair, D.T.Y. Lau, U. Demirci, Enhancing the nanoplasmonic signal by a nanoparticle sandwiching strategy to detect viruses, Appl. Mater. Today. (2020). https://doi.org/10.1016/j.apmt.2020.100709.
15. F. Inci, U. Celik, B. Turken, H.Ö. Özer, F.N. Kok, Construction of P-glycoprotein incorporated tethered lipid bilayer membranes, Biochem. Biophys. Reports. (2015). https://doi.org/10.1016/j.bbrep.2015.05.012.
16. E.M. Burd, Validation of laboratory-developed molecular assays for infectious diseases, Clin. Microbiol. Rev. (2010). https://doi.org/10.1128/CMR.00074-09.
17. Y. Shen, T. Bin Anwar, A. Mulchandani, Current status, advances, challenges and perspectives on biosensors for COVID-19 diagnosis in resource-limited settings, Sensors and Actuators Reports. (2021). https://doi.org/10.1016/j.snr.2021.100025.
18. E. Morales-Narváez, H. Golmohammadi, T. Naghdi, H. Yousefi, U. Kostiv, D. Horák, N. Pourreza, A. Merkoçi, Nanopaper as an Optical Sensing Platform, ACS Nano. (2015). https://doi.org/10.1021/acsnano.5b03097.
19. N. Granqvist, A. Hanning, L. Eng, J. Tuppurainen, T. Viitala, Label-enhanced surface plasmon resonance: A new concept for improved performance in optical biosensor analysis, Sensors (Switzerland). (2013). https://doi.org/10.3390/s131115348.
20. A. Mataji-Kojouri, M.O. Ozen, M. Shahabadi, F. Inci, U. Demirci, Entangled Nanoplasmonic Cavities for Estimating Thickness of Surface-Adsorbed Layers, ACS Nano. (2020). https://doi.org/10.1021/acsnano.0c02797.
21. R. Ahmed, M.O. Ozen, M.G. Karaaslan, C.A. Prator, C. Thanh, S. Kumar, L. Torres, N. Iyer, S. Munter, S. Southern, T.J. Henrich, F. Inci, U. Demirci, Tunable Fano-Resonant Metasurfaces on a Disposable Plastic-Template for Multimodal and Multiplex Biosensing, Adv. Mater. (2020). https://doi.org/10.1002/adma.201907160.
22. E. Bellas, T.J. Lo, E.P. Fournier, J.E. Brown, R.D. Abbott, E.S. Gil, K.G. Marra, J.P. Rubin, G.G. Leisk, D.L. Kaplan, Injectable Silk Foams for Soft Tissue Regeneration, Adv. Healthc. Mater. (2015). https://doi.org/10.1002/adhm.201400506.
23. P. Tseng, S. Zhao, A. Golding, M.B. Applegate, A.N. Mitropoulos, D.L. Kaplan, F.G. Omenetto, Evaluation of Silk Inverse Opals for "smart" Tissue Culture, ACS Omega. (2017). https://doi.org/10.1021/acsomega.6b00320.
24. H. Tao, M.A. Brenckle, M. Yang, J. Zhang, M. Liu, S.M. Siebert, R.D. Averitt, M.S. Mannoor, M.C. McAlpine, J.A. Rogers, D.L. Kaplan, F.G. Omenetto, Silk-based conformal, adhesive, edible food sensors, Adv. Mater. (2012). https://doi.org/10.1002/adma.201103814.
25. F. Inci, M.O. Ozen, Y. Saylan, M. Miansari, D. Cimen, R. Dhara, T. Chinnasamy, M. Yuksekkaya, C. Filippini, D.K. Kumar, S. Calamak, Y. Yesil, N.G. Durmus, G. Duncan, L. Klevan, U. Demirci, A Novel On-Chip Method for Differential Extraction of Sperm in Forensic Cases., Adv. Sci. (Weinheim, Baden-Wurttemberg, Ger. 5 (2018) 1800121. https://doi.org/10.1002/advs.201800121.
26. S.K. Vashist, E.M. Schneider, E. Lam, S. Hrapovic, J.H.T. Luong, One-step antibody immobilization-based rapid and highly-sensitive sandwich ELISA procedure for potential in vitro diagnostics, Sci. Rep. (2014). https://doi.org/10.1038/srep04407.
27. N.G. Welch, J.A. Scoble, B.W. Muir, P.J. Pigram, Orientation and characterization of immobilized antibodies for improved immunoassays (Review), Biointerphases. (2017). https://doi.org/10.1116/1.4978435.
28. K. Lodewijks, W. Van Roy, G. Borghs, L. Lagae, P. Van Dorpe, Boosting the figure-of-merit of LSPR-based refractive index sensing by phase-sensitive measurements, Nano Lett. (2012). https://doi.org/10.1021/nl300044a.
29. H.J. Weeth, R. Witton, C.F. Speth, Prediction of Bovine Urine Specific Gravity and Total Solids by Refractometry, J. Anim. Sci. (1969). https://doi.org/10.2527/jas1969.28166x.
30. S. Liu, Z. Deng, J. Li, J. Wang, N. Huang, Measurement of the refractive index of whole blood and its components for a continuous spectral region, J. Biomed. Opt. (2019). https://doi.org/10.1117/1.jbo.24.3.035003.
31. Y. Zhuo, H. Hu, W. Chen, M. Lu, L. Tian, I.M. Carreira, K.D. Long, E. Chow, W.P. King, S. Singamaneni, B.T. Cunningham, Single nanoparticle detection using photonic crystal enhanced microscopy, Analyst. (2014). https://doi.org/10.1039/c3an02295a.
32. G. Li, X. Li, M. Yang, M.M. Chen, L.C. Chen, X.L. Xiong, A gold nanoparticles enhanced surface plasmon resonance immunosensor for highly sensitive detection of Ischemia-modified albumin, Sensors (Switzerland). (2013). https://doi.org/10.3390/s131012794.
33. Ö. Erdem, E. Derin, K. Sagdic, E.G. Yilmaz, F. Inci, Smart materials-integrated sensor technologies for COVID-19 diagnosis, Emergent Mater. (2021). https://doi.org/10.1007/s42247-020-00150-w.
34. Ö. Erdem, I. Eş, G.A. Akceoglu, Y. Saylan, F. Inci, Recent advances in microneedle-based sensors for sampling, diagnosis and monitoring of chronic diseases, Biosensors. (2021). https://doi.org/10.3390/bios11090296.